Random field modelling of mechanical behaviour of corroded thin steel plate specimens

Krzysztof Woloszyk[a], Yordan Garbatov[b, 1]

[a] Faculty of Ocean Engineering and Ship Technology, Gdansk University of Technology,
G. Narutowicza 11/12 st., 80-233 Gdansk, Poland
[b] Centre for Marine Technology and Ocean Engineering (CENTEC), Instituto Superior Técnico,
Universidade de Lisboa, Avenida Rovisco Pais 1049-001 Lisboa, Portugal

Abstract

The objective of this work is to explore the possibility of corrosion degradation modelling of thin steel plate specimens with the use of random field approach. The mechanical properties are obtained via the nonlinear Finite Element Analysis with the use of an explicit dynamic solver. The fully nonlinear material model is adopted to obtain the proper stress-strain response. Sensitivity analysis considering the main statistical descriptors of the random field is performed. The results of the analysis are validated with the available experimental data showing a good agreement for lower levels of Degree of Degradation and significant deviations for severely corroded specimens. The analysis shows that the irregularities in the corroded plate surface are one of the main reason for the mechanical properties reduction. Random field modelling revealed to be a swift and practical tool for representing the corroded surfaces in steel structures.

Keywords: Corrosion, Mechanical Properties, Finite Element Method, Random Field

1. Introduction

Many steel structures operate in different marine environmental conditions subjected to corrosion degradation [1]. In the last decades, various models of thickness reduction due to corrosion were developed [1–3]. Recently attention was paid to the fact that not only thickness reduction concerning corrosion is observed, but also mechanical properties changes are observed as well [4] leading to severe strength reduction [5–9].

The discussion about the reduction of mechanical properties of steel specimens with the subsequent corrosion degradation is vital. During the last couple of years, several studies have been done, mainly experimentally, but also in the numerical domain. Garbatov et al. [4] tested corroded plate specimens with different corrosion severity. They concluded that for the specimens with degradation level higher than 20%, the mechanical properties reduction is significant. Not only yield strength, and the Young modulus is reduced, but also the elongation is significantly reduced. Kashani et al. [10] analysed the stress-strain behaviour of non-uniformly corroded steel circular bars. In this case, the degree of degradation was up to 20%. The reduction of yield strength was up to 30 % and the reduction of the mean strain at failure was even up to 80 %. Zhan et al. [11] tested 267 corroded steel bars that were corroded in different conditions (in a laboratory and natural environment). They concluded that the

---

[1] Corresponding author e-mail: yordan.garbatov@centec.tecnico.ulisboa.pt; Telf (351) 21 841 7907

mechanical properties are significantly deteriorated, and the yield plateau of the steel bar became shorter or even disappeared with the development of the corrosion. In the study performed by Fernandez and Berrocal [9], 30-years old, naturally corroded steel reinforcing bars where examined. Beside the tensile tests, they measured the corrosion distribution along the bars. They concluded that the reduction of the mechanical properties is governed by the minimal cross-section area of the specimen. Additionally, Li et al. [12,13] performed the tensile test of pre-stressed and corroded specimens, and the effect of the mechanical properties reduction was magnified with comparison to only corroded specimens.

In case of the ship and offshore structures, thin-walled structures such as plates and slender beam are more often used. The mechanical properties of corroded flat specimens were investigated in [14–18], and the conclusions were similar to those obtained for bars. The reduction was observed not only in severe corrosion conditions but also in lower corrosion degradation. In the case of very thin plates, such as one millimetre of thickness, the reduction of the mechanical properties was up to 70% from their initial values [15].

Most researchers agreed that if the corrosion is uniform, it would not have a significant effect on the mean stress-strain response. Thus induce, that the reduction of mechanical properties is caused by the non-uniform distribution of corrosion pits [19–22]. This hypothesis is supported by experimental results of Garbatov et al. [23], where specimens after cleaning showed higher values of mechanical properties compared to corroded non-cleaned ones. In the case of the marine environment and especially for ships structures, the non-uniform corrosion is the most common one, and this phenomenon cannot be neglected.

Based on the experimental results, several mathematical models for the prediction of mechanical properties of corroded bars and flat specimens were developed [24,25]. Li et al. [26] developed a simplified constitutive model for corroded bars based on experimental and numerical studies. Garbatov et al. [4] developed a model for corroded coupon specimens. Other mathematical models for estimation of different mechanical properties of flat bars that are based on experimental investigations can be found in [27–30]. Although couple models were developed, it seems that more work is still needed towards in developing a more unified approach with regards to mechanical properties change in terms of corrosion degradation.

With the development of more advanced measuring techniques, the detailed measurements of 3D corrosion morphology are possible. Examples of such measurements can be found in [31–33]. Based on that, the mechanical properties of corroded specimens or fatigue properties can be evaluated [33–35] and even the structural response of beam elements may be analysed [36]. Wang et al. [14] compared some experimental results with the nonlinear FE analysis, where the corrosion surface was scanned and implemented in the finite element model. The agreement between experimental and numerical results was good.

Based on the data collected about mechanical properties changes [37], a numerical model of corroded structures can be developed, such as presented in [38]. In this case, the ultimate strength of corroded stiffened plates was evaluated and compared to the experimental results reported in [39]. However, in this case, the degree of degradation levels was very high (above 40 %). Usually, the plates with that levels of corrosion are replaced in real structures. The study presented in the sections explores the mechanical properties change with lower levels of degradation.

Due to the complexity of methods for measurements of different structural imperfections, such as corrosion degradation, initial distortions etc., the random field modelling [40] seems to be a powerful tool for the modelling of such imperfections. The examples of random field modelling to reflect the

geometric and material imperfections can be found in [41–43]. The possibility of stochastic modelling of corrosion field was also presented in [44]. Additionally, the random field approach can provide many samples which are usually hard to obtain, especially for relatively large structures such as ships or offshore platforms. Thus, it can be exploited in the reliability analysis [45].

In the presented study, the random field approach is applied in modelling corroded surfaces to evaluate the mechanical properties of corroded specimens subjected to general corrosion. The nonlinear FE method with the use of the explicit dynamics solver is used. The sensitivity analysis concerning the governing factors of the random field is performed. The results of experimental investigations presented in [15] are used to validate the present study.

2. Corrosion degradation modelling using random field

Due to the natural origin of the corrosion environment, the surface of the corroded plate can be modelled with the use of a random field. The spatial distribution of corrosion pits may be modelled by the random field approach as the one that is the most suitable for this purpose, due to the set of an infinite number of spatially correlated random variables. For engineering purposes, one needs to find a random field with a finite number of random variables, and with this respect, the Gaussian random field can be defined entirely by its mean $\mu(\boldsymbol{x})$, variance $\sigma^2(\boldsymbol{x})$ and autocovariance function $C(\boldsymbol{x}, \boldsymbol{x}')$.

Different discretisation methods of the random field are available. In the present study, the Karhunen – Loeve expansion [46] is used to simulate the random field for a specific mesh density. Other discretisation methods may be found in [46,47]. The Karhunen – Loeve expansion is widely used in stochastic Finite Element methods due to some useful properties, including the positive covariance matrix, a limited number of random variables and it is undoubtedly convergent. According to this expansion method, the random field can be expressed as follows:

$$H(\boldsymbol{x}, \theta) = \mu(\boldsymbol{x}) + \sum_{i=1}^{\infty} \sqrt{\lambda_i}\, \xi_i(\theta) f_i(\boldsymbol{x}) \tag{1}$$

where λ_i and $f_i(\boldsymbol{x})$ are the eigenvalues and eigenvectors of the covariance function $C(\boldsymbol{x}, \boldsymbol{x}')$, where $\boldsymbol{x}$ and $\boldsymbol{x}'$ are two coordinates defined for a specific mesh density. In the case of the random field defined in a 2D surface, each vector will consist of two components.

The parameter $\xi_i(\theta)$ is defined as a set of uncorrelated random variables with a mean value and covariance function of:

$$E[\xi_i(\theta)] = 0 \tag{2}$$

$$E[\xi_i(\theta)\xi_j(\theta)] = 1 \tag{3}$$

Assuming that $H(\boldsymbol{x}, \theta)$ is a zero-mean Gaussian process, $\{\xi_1(\theta), \xi_2(\theta), \dots\}$ is a vector of uncorrelated random variables sampled from a zero-mean normal distribution.

Truncating the series from Eq. 1 after the nth term, one can obtain an approximated solution of $H(\boldsymbol{x}, \theta)$:

$$\widehat{H}(\boldsymbol{x}, \theta) = \mu(\boldsymbol{x}) + \sum_{i=1}^{N} \sqrt{\lambda_i}\, \xi_i(\theta) f_i(\boldsymbol{x}) \tag{4}$$

The corresponding autocovariance function is given by:

$$\widehat{C_{HH}}(\boldsymbol{x}, \boldsymbol{x}') = \sum_{i=1}^{N} \sqrt{\lambda_i}\, f_i(\boldsymbol{x})\, f_i(\boldsymbol{x}') \qquad (5)$$

When the mean value and variance are constant, the autocovariance function depends only on an absolute distance between points x and x', the field is homogenous. Different types of autocovariance function can also be used. In the presented study, the square exponential autocovariance is used:

$$C(\boldsymbol{x}, \boldsymbol{x}') = \exp\left(\frac{(\boldsymbol{x} - \boldsymbol{x}')^2}{c_0^2}\right) \qquad (6)$$

where $(\boldsymbol{x} - \boldsymbol{x}')$ is the absolute distance and c_0 is the correlation length (also known as a damping parameter). The correlation length is the most influencing parameter changing the spatial variation of the field. When c_0 increases, the correlation is extended, and the field becomes smoother, and when c_0 decreases, the correlation is reduced, and the field is more irregular. The example of different level of correlated fields is presented in Figure 1, where the fields are with an identical mean value and variance, but different correlation lengths.
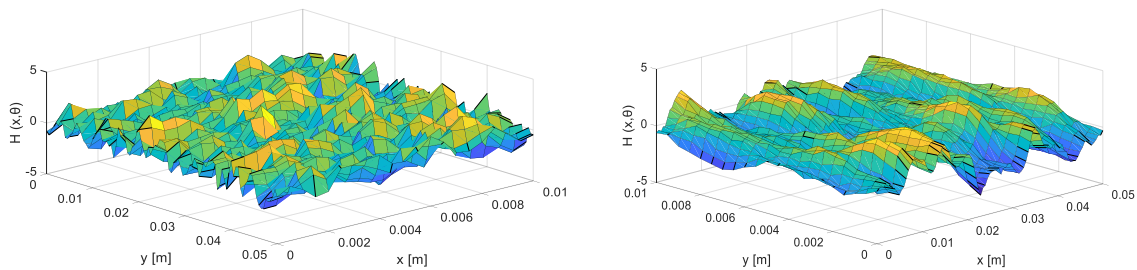

Figure 1. Random field with reduced (left) and extended (right) correlation.

The random fields are generated with the use of MatLab software [48] and specially developed code [49], which allow generating a Gaussian random field for a specified mesh density and different correlation lengths. The calibration of the correlation length is based on the real corrosion degradation measurements.

However, as can be seen in some studies such as in [14], where detailed measurements of the corroded surface were carried out, the maximum corrosion depth is much higher than the mean value, which leads to the log-normal distribution of the corrosion depth. For proper modelling, the normal field is transformed into a log-normal field in the case of the present study as:

$$L(\boldsymbol{x}) = \exp\big(\mu + \sigma H(\boldsymbol{x})\big) \qquad (7)$$

where μ and σ are the scaling parameters of the log-normal field, and they are calibrated to produce a proper mean value and standard deviation of the random field. The example of the random field transformation is presented in Figure 2. The normal random field is with a zero mean value and variance equal to one. The scaling parameters of the log-normal distribution are equal to zero and 0.5, respectively. It can be noticed that negative values of the normal field are flattened in the log-normal field, whereas positive values are sharpened.
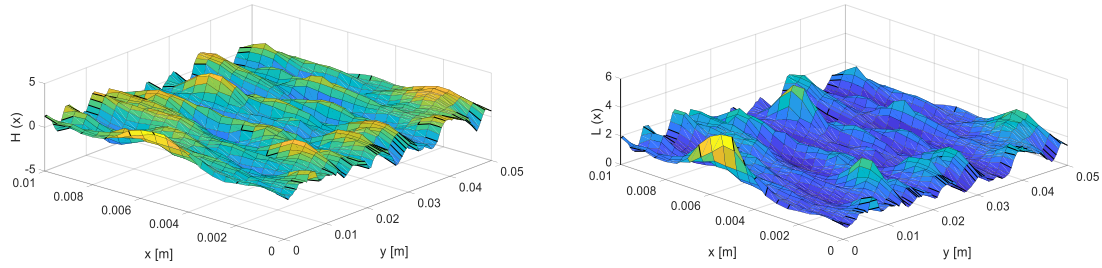
Figure 2. Normal (left) and log-normal (right) random field.

The statistical descriptors presented in this study will be calibrated based on the experimental results [15] examining the feasibility of the proposed methodology here. However, the random field of the corroded plate surface can be generated for the assumed standard deviation and mean value of the corrosion depth.

3. Finite Element modelling

To analyse the mechanical behaviour of the tensile tested steel specimen, ANSYS LS-DYNA [50] software is used. As an input stress-strain relationship of mechanical properties, the multilinear true stress-strain curve is applied, and the specimen is modelled with the use of SOLID164 elements for explicit dynamics. The element fractures, when the strain reaches the failure strain. Nevertheless, the tensile test is quasi-static, the explicit dynamics solver is used to overcome the convergence difficulties [51], which is a very known problem for this type of analysis [52]. The convergence difficulties, in this case, are originated both from the necking phenomenon during the testing process as well as corrosion pits, which produce high nonlinearities. During the tensile test, one can obtain the so-called engineering stress-strain curve, which is typically required by standards for tensile testing [53], i.e. the stress is calculated as force divided by initial cross-sectional area and strain is calculated as the longitudinal displacement divided by the initial length of the specimen. However, in the FE model, the true stress-strain curve is applied. The true strain and true stress are given as [54]:

$$\varepsilon_{true} = \ln(1 + \varepsilon) \tag{8}$$

$$\sigma_{true} = \sigma(1 + \varepsilon) \tag{9}$$

where σ and ε are engineering stress and strain, respectively.

It occurs, that these equations are true up to the ultimate point, after that the necking phenomenon in ductile steels starts and to account for that a procedure based on the power law is applied [55]:

$$\sigma_{true} = K\varepsilon_{true}^n \tag{10}$$

where K and n are the strength coefficient and strain hardening parameter, respectively. Both of these values and additionally, true failure strain is calibrated to obtain the same engineering stress-strain relationship as the one generated during the experiment.
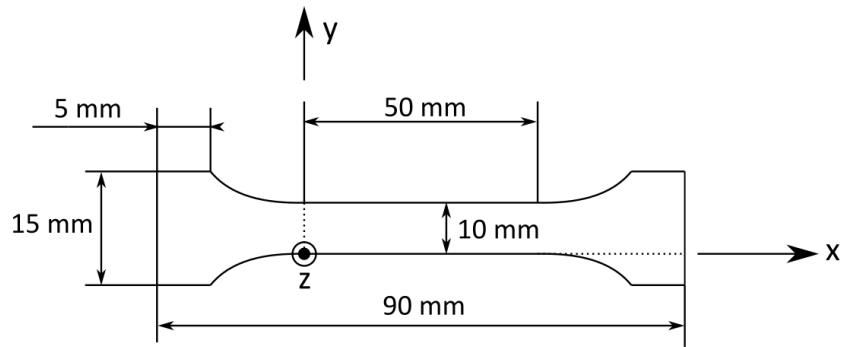
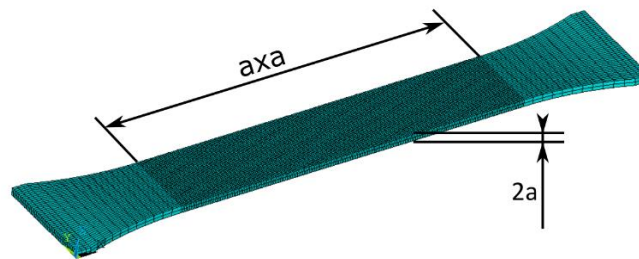Figure 3. Specimen dimensions and system of coordinates.

Figure 4. FE model of the specimen

The specimen dimensions are presented in Figure 3, and the FE model with finite element size distribution is presented in Figure 4, where a is the nominal element size in mm. The gauge field, where the corrosion will be modelled, is of 50 x 10 mm. It can be noticed that the element size in the thickness direction is two times bigger than in longitudinal and transverse directions. This type of mesh density is adopted to decrease the computational time, and in this case, the dense mesh should be applied in the upper surface of the specimen, where the corrosion field will be applied (only one side corrosion degradation is modelled).

Additionally, when the corrosion field is generated, the height of the elements became smaller, and the aspect ratio tends to one for the upper layers of the specimen. The size of elements of support mounting and transitional parts are not so relevant, and there are resulting from the element size in the gauge region in transverse and the thickness direction. In the longitudinal direction, the element size is kept as large as possible to reduce the computational time. The boundary conditions are applied in the region of the support mounting parts. To simulate the experimental conditions, the upper and bottom surfaces of left-side of the mounting part are fixed in all directions (x, y and z), whereas the surfaces of the right-side mounting part are fixed in the y and z-direction, and the longitudinal displacement is applied in the x-direction. The longitudinal displacement is applied incrementally via small time steps using the explicit solver.

Additionally, to the calibration of the stress-strain relationship, the mesh convergence studies are carried out to find the proper element size, which will provide reliable results. The element size a analysed ranged from 0.25 mm up to 2.5 mm, and the mechanical properties are estimated. The results are presented in Figure 5. It can be noticed that all governing parameters get the most accurate values with the refined mesh with an element size of 0.25 mm. It is interesting to point out that a significant difference in the total elongation between the coarse and refined mesh densities is reaching 26 % in the case of a 2.5 mm element size. This may be originated by the complex necking phenomenon, which requires a dense mesh in the necking region to obtain a proper strain distribution in the net cross-section. Further analysis showed that the 0.25 mm element size provides a good representation of the

corrosion field, especially in the case of reduced extension of the correlation. Based on this, 0.25 element size was chosen to model the corroded specimens.

Table 1. Mesh convergence results.

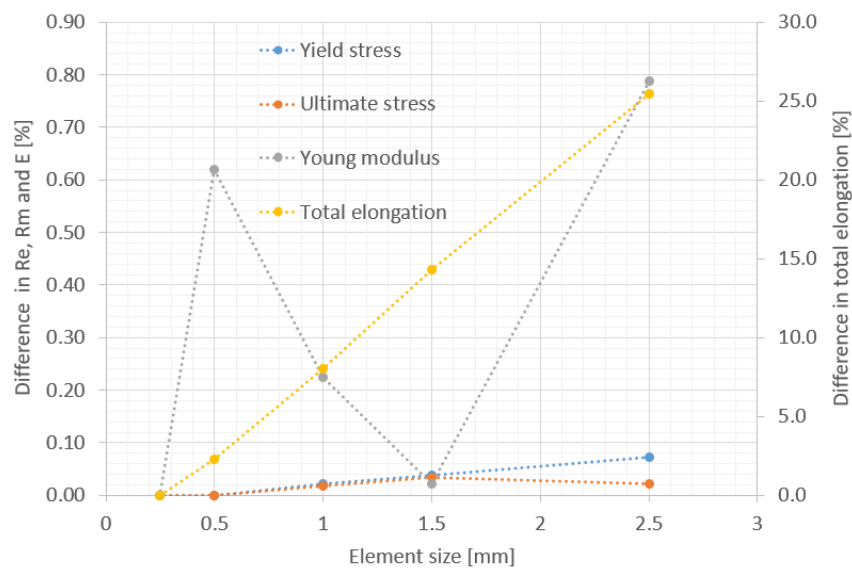| Element size a [mm]	Number of elements [length x width x thickness]	Difference in yield stress [%]	Difference in ultimate stress [%]	Difference in the Young modulus [%]	Difference in total elongation [%]
2.5	20 x 4 x 1	0.07	0.02	0.79	25.5
1.5	33 x 10 x 1	0.04	0.03	0.02	14.3
1	33 x 17 x 2	0.02	0.02	0.22	8.0
0.5	100 x 20 x 2	0.00	0.00	0.62	2.3
0.25	200 x 40 x 2	0.00	0.00	0.00	0.0

Figure 5. Mesh convergence results.

A further analysis is performed for validating the generated model here with the experimental results of Nie et al. [15], and thus, the stress-strain relationship presented in this study is the basis for the current analysis. The primary material properties of referred material (mild steel S235) are yield stress, Young (elasticity) modulus, ultimate stress and total elongation are 287 MPa, 178.5 GPa, 333 MPa and 24.2 %, respectively. The first part of the true stress-strain relationship is established with the use of Eqns 8 and 9 up to the true strain of 0.178, which corresponds to the ultimate strain. The second part of the curve is calibrated with the experimental one using Eqn 10, leading to $\varepsilon_{failure} = 0.74\,[-], K = 550\,MPa, n = 0.19\,[-]$. The comparison between the input stress-strain and output engineering

curve with a comparison of the experimental one is shown in Figure 6. It can be noticed, that FE element stress-strain relationship matches the experimental one and the basic mechanical properties are the same in both cases, although minimal deviations after reaching the ultimate point are visible. Additionally, the strain distribution after failure is shown in Figure 7, where the occurrence of the necking phenomenon, as well as breaking initiation in the middle of the width of the specimen, confirm that the numerical model provides proper results.
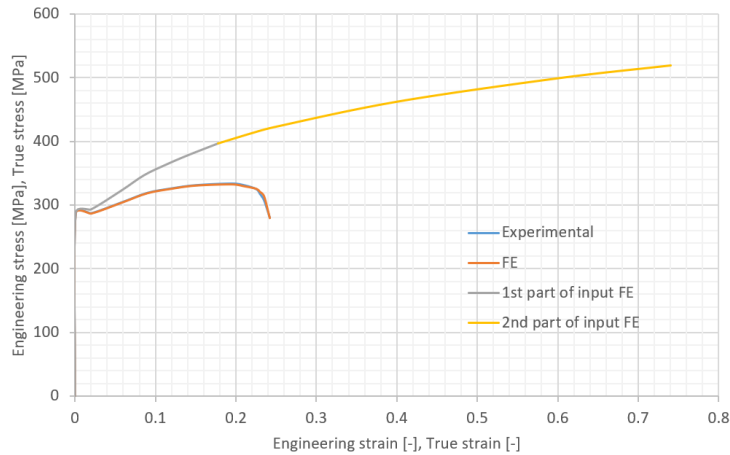

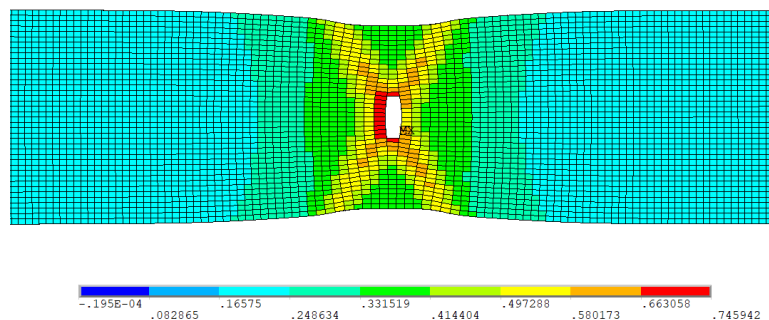Figure 6. Experimentally and numerically developed stress-strain relationships.

Figure 7. Strain distribution in the non-corroded specimen during breaking.

4. Corrosion degradation modelling

The corrosion degradation may be one or two-side developed depending on the environmental conditions and structural component location and position. Since the results of this study are validated with the experimental data of [15], the corrosion is considered as a one-side. In both cases, some corrosion degradation descriptors are distinguished. The approach which is adopted in the present study is presented in Figure 9, where a typical cross-section of the corroded specimen with a randomly generated corrosion field as presented in Figure 8. The initial thickness t_0 is the as-built thickness of corroded specimen and t_{max} is the maximum residual corroded plate thickness. The difference between those two variables divided by the initial thickness is the uniform degree of degradation:

$$DoD_u = \frac{t_0 - t_{max}}{t_0} \tag{11}$$

In the upper surface, corrosion degradation creates an irregular field. The corrosion depth of any particular point in the upper surface is h, and it is the difference between the maximum residual

thickness of the corroded specimen t_{max} and the thickness at this point t. One can distinguish the maximum corrosion depth, Δh, as well as mean value, $\bar{h}$. The minimum thickness is taken as:

$$t_{min} = t_{max} - \Delta h \qquad (12)$$

The non-uniform degree of degradation is calculated by integrating the total volume of the corroded specimen, $V_{corroded}$, and it is equal to:

$$DoD_n = \frac{t_{max} \cdot A - V_{corroded}}{t_0 \cdot A} \qquad (13)$$

The total degree of degradation then is equal to:

$$DoD = DoD_u + DoD_n \qquad (14)$$

Additionally, by calculating the cross-sectional areas of the corroded specimen A_i (presented in Figure 8 in red colour) along with the specimen, the minimum cross-sectional area A_{min} can be obtained.
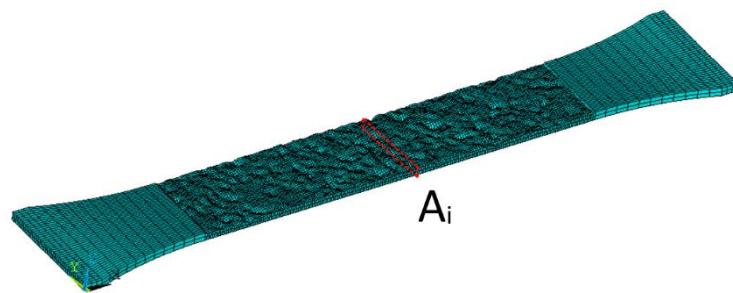

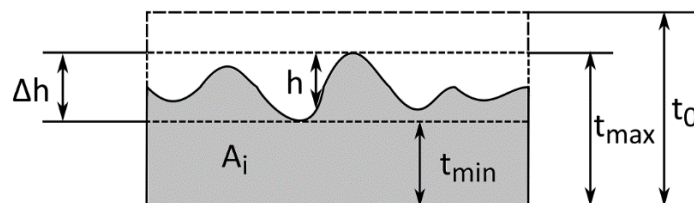Figure 8. FE model of the corroded specimen.

Figure 9. Cross-section of corroded specimen.

The maximum corrosion depth, together with the mean corrosion depth and correlation length, are the three parameters that define the random corroded field. Each discretised random field is generated for a particular mesh density, and then it is transformed into an FE model by changing the z-coordinate of any particular nodes, keeping the lower surface intact. However, to avoid excessive skewness of finite solid elements, not only the very top surface is modified but also the one surface below is transformed. The z-coordinate of each node in the surface below the top one is transformed by half of the corrosion depth of the top surface, as shown in Figure 10.
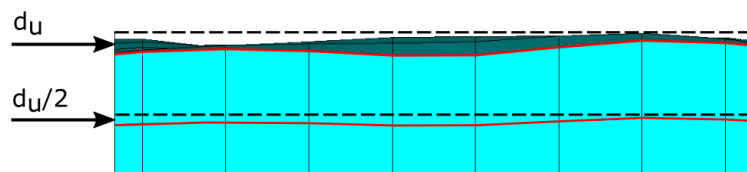

Figure 10. FE corrosion modelling.

One can choose different corrosion descriptors as a reference value for the mechanical properties estimation, i.e. the average thickness, maximum thickness, minimum cross-sectional area, initial thickness etc. Only detailed measurements of the mass and detailed scanning of cleaned specimens can provide reliable information to identify the corrosion degradation descriptors. However, in real operational conditions, such measurements are impossible. Due to that, the maximum residual thickness, t_{max}, is chosen to be a governing factor in the reduction of mechanical properties. Since the proposed model is developed to be used for real structures, the most common factor for identifying the severity of the degradation is the residual thickness during service life employing the ultrasonic method [56]. In the study presented in [57] an analysis of ultrasonic measurements for the rough surface in the back wall of the analysed specimen is shown (a situation was very often seen during inspections). The output is subjected to a high level of uncertainties, which is magnified with the irregularities of the corroded surface. Additionally, they showed that the ultrasonic method tends to show higher values of thickness compared to average corroded plate thickness. Since this method is used in measurements of structures during service life, it seems more reasonable to take the maximum residual thickness as a reference factor in the estimation of mechanical properties.

In the case of ships, designed according to Classification Societies Rules [58], all the plates and stiffeners are designed with an addition identified as a corrosion addition. All structural members without corrosion additions should satisfy the strength requirements. The plate thicknesses are measured during service life to ensure that the thickness reduction is not more than the corrosion addition.

5. Sensitivity analysis

To establish the most influencing parameters in the random field generation, the global sensitivity analysis is performed. The analysed random field parameters are presented in Table 2. The ratio between the maximum and mean corrosion depth varies between 2 and 5. By changing the maximum corrosion depth to the mean corrosion depth, the shape of the random field will change. With a higher corrosion depth, the field will be sharper. In this way, the variance of the random field is calibrated to obtain the same maximum thickness value and minimum cross-sectional area. The standard deviation for the random field varies between 0.039 mm and 0.053 mm for the highest value of the ratio between the maximum and mean corrosion depth. The correlation length varies between 0.3 and 1.0. When correlation length is less than the element size, the two points of mesh grid are in fact non-correlated. Thus, the minimum of the correlation length is taken as 0.3 mm. The initial thickness of the intact plate is 1 mm. In each case, the maximum thickness and minimum cross-sectional area are the same, and there are equal to 1 mm and 8 mm^2 respectively. The input stress-strain relationship of the analysis is presented in Figure 6.

Table 2. The design values of sensitivity analysis.

Variable	Initial	Minimum	Maximum
Maximum corrosion depth/ Mean corrosion depth [-]	3	2	5
Correlation length [mm]	0.5	0.3	1.0

The sensitivity analysis is performed using OFAT (one factor at the time) methodology [59], i.e. only one parameter is changed from its initial value, where the others are fixed. Although the more advanced techniques of Design of Experiments [60] can be used, this type of analysis can provide information about relevant and irrelevant variables in a quite straightforward way, which is the purpose of the current analysis. Due to that, some variables may be excluded from the later analysis

and the multi-factorial analysis may be performed to show the interaction between factors. The results of the analysis are presented in Table 3. For each correlation length, five runs with different realizations of the random field were performed. The coefficient of variation of each variable was presented in the brackets together with the mean value. It could be noticed, that the yield and ultimate stress are not very dependent on the number of realisations. In the case of Young modulus and total elongation, the scatters are significant. Additionally, the variance of the total elongation is increasing with the increase of the correlation length.

Table 3. Results of sensitivity analysis.

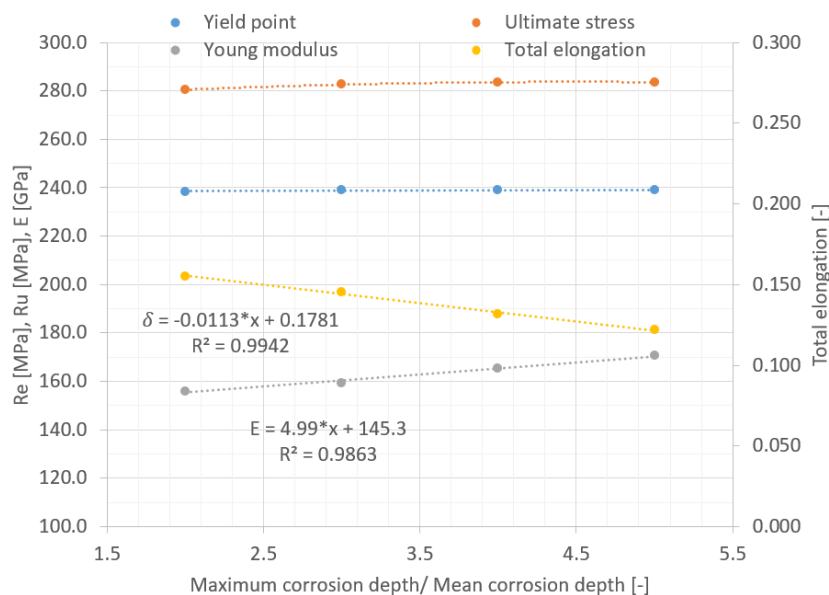| Influencing factor	Value	Re [MPa]	Ru [MPa]	E [GPa]	δ [-]
Maximum corrosion depth/ Mean corrosion depth [-]	2	238.3	280.5	156.0	0.155
	3	239.0	282.6	159.2	0.145
	4	238.9	283.6	165.5	0.131
	5	238.9	283.6	170.5	0.122
Correlation length [mm] (COV [%])	0.3	228.6 (0.7)	273.2 (0.5)	147.0 (6.8)	0.152 (4.2)
	0.4	229.7 (0.6)	274.9 (0.5)	141.8 (4.3)	0.153 (6.5)
	0.5	234.1 (2.1)	278.0 (1.6)	157.2 (2.9)	0.139 (6.3)
	0.75	231.9 (1.4)	275.0 (1.1)	158.0 (8.3)	0.123 (17.4)
	1.0	231.3 (1.6)	271.6 (1.1)	180.5 (9.3)	0.097 (16.1)

Figure 11. Mechanical properties as a function of corrosion depth ratio.

Figure 11 shows the influence of the ratio between maximum and mean corrosion depth in the mechanical properties of corroded specimens. It can be noticed that the yield and ultimate stresses are not sensitive to this parameter. The influence of the ratio between maximum and mean depth is visible in the case of the total elongation and Young modulus. In both cases, the linear approximation functions are with the highest correlation factor. When the ratio is increasing, the Young modulus increases as well, whereas total elongation is decreasing. The differences between maximum and minimum values for these two variables are in the order of 9 % in the case of the Young modulus and in the order of 21 % in the case of the total elongation.
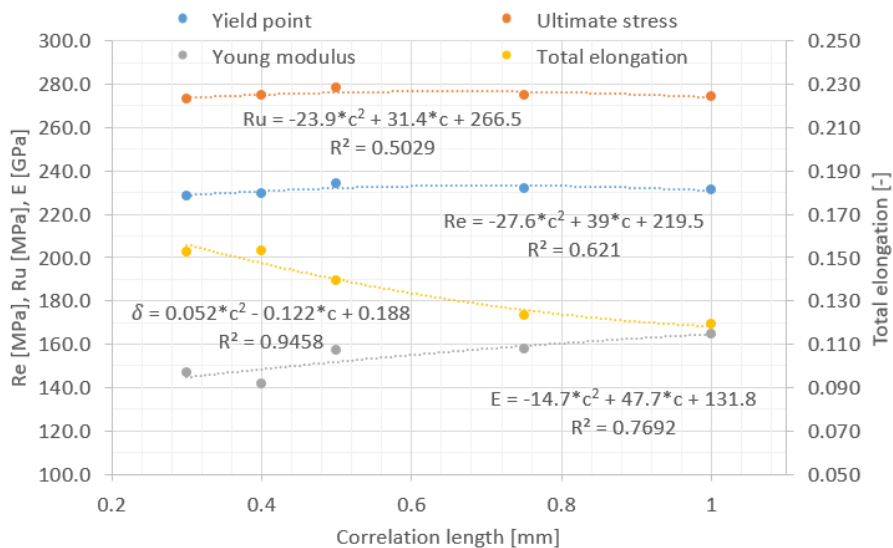
Figure 12. Mechanical properties as a function of the correlation length.

Figure 12 shows the impact of the correlation length of the random field on the mechanical properties. The correlation length has almost no influence on both yield and ultimate stresses (the differences between the maximum and minimum values are in the order of 4%). The significant impact is seen in the case of the Young modulus (difference of 19% between the maximum and minimum value) and total elongation (difference of 25 %). For all variables, the second polynomial regression functions are found to have the highest correlation factor. In the case of yield and ultimate stresses, the correlation factor is quite low, and it can be concluded that the deviations are of a stochastic origin. However, in the case of the Young modulus and total elongation, the correlation factors are significant. When the correlation length is extended, the Young modulus is also growing, and the total elongation is reduced.

The results may deviate due to the different realisations of the random field with the same statistical descriptors. Thus, for the specific correlation length and ratio between maximum and mean corrosion depth, the mechanical properties may be slightly higher or lower between different realisations of statistically identical random fields. It can be noticed that the total elongation is subjected to high uncertainties. The total elongation is dependent on any specific corroded surface field, which can be seen in different failure schemes (Figure 13) for specimens with different correlation lengths. Generally, the reduction of the total elongation is related to premature breaking due to the stress concentration in the region of the deep pit, which can be visible in the strain distribution of the corroded specimen. It can also be noticed that the breaking line is not perpendicular to the longitudinal direction of the specimen, and the breaking can also not be located in the middle-length of the specimen.
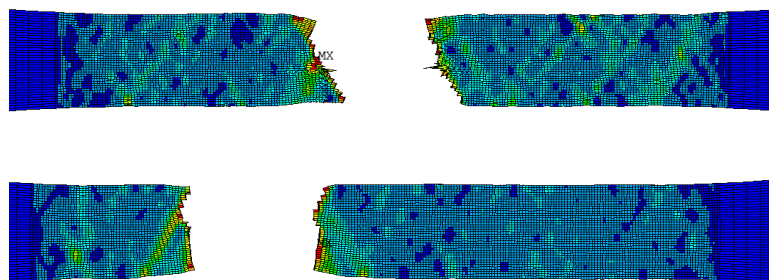

Figure 13. Failure of specimens in case of correlation length equal to 0.4 mm (up) and 0.5 mm (bottom).

Based on the sensitivity analysis, one can conclude, that correlation length and the ratio between the maximum and mean corrosion depth are influencing the reduction of mechanical properties when corrosion field is modelled with the use of random field approach. The most sensitive variables are the total elongation and Young modulus, and additionally, there are subjected to higher uncertainties with comparison to yield and ultimate stresses. Yield and ultimate stresses are not so sensitive for the change of the random field parameters, and it can be concluded that there are mostly dependent on the minimum cross-sectional area.

6. Finite element analysis of corroded specimens

The corrosion field, modelling with the use of the random approach, is compared to experimental results of very thin plates as reported in [15] (the initial thickness is 1 mm). Seven specimens were cut from a real structure and exposed to atmospheric corrosion conditions. However, only the maximum residual thickness and minimum cross-sectional area are provided as a result of the corrosion morphology analysis. The corrosion is one-side in this case. The dimensions of the gauge area of the specimens are 50x10 mm, and the specimen dimensions are identical as presented in Figure 3. The initial stress-strain relationship is calibrated, as presented in Figure 6. Based on the corrosion morphology results, one can notice that the correlation is higher for severely corroded specimens. However, due to a lack of specific information of the corrosion field correlation, the correlation length of 0.6 mm is assumed for higher values of DoD (above 15 %), and correlation length of 0.4 mm is assumed for lower values of DoD (below 15 %). In this way, the corrosion fields are similar to those obtained in the experiment. The comparison between real corrosion field and randomly generated one for a low value of DoD is presented in Figure 14. The ratio between the maximum corrosion depth to mean corrosion depth was taken as 3 in this case. Due to the lack of mass measurements, the degree of degradation is calculated as a ratio between the minimum cross-sectional area to the initial cross-sectional area. Normally, the DoD values will be higher. The maximum residual thickness and minimum cross-sectional area are the same in the experimental domain and numerical model, as presented in Table 4.

Table 4. Specimens description.

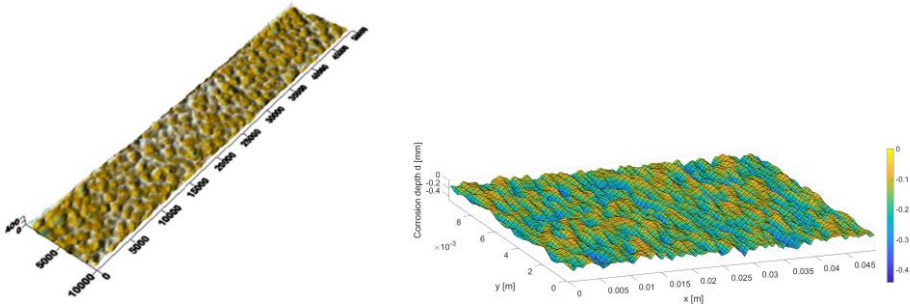| Specimen	t_{max} [mm]	A_{min} [mm^2]	DoD [%]
F1	1.00	8.474	12.1
F2	1.01	9.006	6.6
F3	0.95	7.766	19.5
F4	1.00	8.32	13.7
F5	0.89	6.326	34.4
F6	0.85	5.94	38.4

Figure 14. Corrosion field in experiment (left) and randomly generated (right).

The results of the analysis are presented in Table 5 and Figures 16 and 17. For each pair of experimental and numerical results, the relative error concerning the experimental one is presented.

Table 5. Results of analysis.

No	R_e [MPa] [15]	R_e [MPa] num.	Error [%]	R_u [MPa] [15]	R_u [MPa] num.	Error [%]	E [GPa] [15]	E [GPa] num.	Error [%]	δ [-] [15]	δ [-] Num.	Error [%]
F0	286.9	286.9	-	333.4	333.4	-	178.5	178.5	-	0.242	0.242	-
F1	258.7	245.0	5.3	292.2	291.3	0.3	155.1	154.8	0.2	0.188	0.178	5.4
F2	263.0	255.0	3.1	311.3	300.7	3.4	168.7	159.8	5.3	0.217	0.190	12.4
F3	195.7	238.7	22.0	223.9	283.2	26.5	127.6	156.9	23.0	0.082	0.120	46.3
F4	215.3	240.3	11.6	254.4	286.7	12.7	150.1	152.4	1.5	0.136	0.166	22.2
F5	105.9	207.3	95.8	113.9	245.5	115.6	99.5	138.9	39.6	0.034	0.068	99.5
F6	79.8	203.6	155.2	92.9	240.7	159.2	97.2	138.1	42.1	0.019	0.061	223.3

Based on the presented results, it can be noticed that in the range between 0 % up to 15 % of DoD the numerical predictions are quite similar to experimental results (F1, F2 and F4 specimen). The deviations can be originated from fluctuations of mechanical properties itself [61]. However, for higher DoD values, the differences are very significant (F3, F5 and F6 specimen). Probably in the case of very thin plates, not only the geometrical deviations of the corrosion field will cause the mechanical properties reductions. The reduction of mechanical properties is very significant, especially for high values of DoD. In the case of the numerical predictions, the mechanical properties (yield stress and ultimate stress) cannot be lower than those, when we consider only the minimum thickness as residual material of specimen. Additionally, their reduction will be lower than this value. In this case, the maximum possible reduction can be calculated as equal to $1 - t_{min}/t_{max}$. The reduction should be below this value and above 0. In Table 6, the reductions in the experimental and numerical analyses concerning the maximum possible reductions are presented. It can be noticed, that in the case of F1, F2 and F4 specimens, the reductions of yield and ultimate stresses are below the maximum possible level in both numerical and experimental domains. In the case of F3, F5 and F6 specimens, the reductions in the experiments are above the maximum possible level or almost equal to it, whereas in the numerical calculations there are below this level. This led to the conclusion that for very thin plates, general corrosion morphology is not the only factor that governs mechanical properties reduction. Very irregular breaking shapes can be observed for severely corroded specimens such as presented in Figure 15. Possibly, this type of breaking can be observed in the numerical model, where tiny element size will be applied (about 0.1 mm or even smaller) and significantly increases the computational time. For this order of the element size, the lower correlation length values can be possibly applied, and more localised phenomena will be observed. This will result in higher levels of stress concentration factors in the pitted regions and possible a higher reduction of mechanical properties. The other possible reason for the significant deviations can be the changes in the microstructure of steel, which cannot be captured by modelling of the corroded surface.
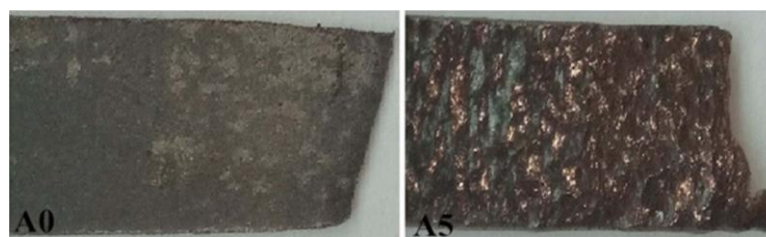

Figure 15. Comparison between non-corroded and severely corroded specimen [15].

Table 6. Reductions of yield stress and ultimate stress.

Specimen	Maximum possible reduction [%]	R_e red. exp. [%]	R_e red. num. [%]	R_u red. exp. [%]	R_u red. num. [%]
F1	34	10	15	12	13
F2	25	8	11	7	10
F3	35	32	17	33	15
F4	37	25	16	24	14
F5	55	63	28	66	26
F6	57	72	29	72	28

Figure 16 presents the yield stress as a function of DoD. Both numerical and experimental curve can be modelled with the use of a linear relationship. However, the significant deviations between them can be observed mainly as a result of deviations for the high values of DoD (above 20%). In the case of DoD up to 15 %, the deviations are in the range of the initial mechanical properties variability. Very similar observations can be seen in the case of the ultimate stress (Figure 16 right).

The Young modulus as a function of DoD is presented in Figure 17. In this case, the deviations in the range between 0 % and 15 % of DoD are even smaller than in the case of the yield and ultimate stress. However, similarly to these two variables, the very significant deviations are for the DoD above 20 %.

Figure 17 also shows the total elongation as a function of DoD. Apart from that the relative deviations between the two approaches are higher as presented in Table 11, the inclination of curves seems to be more closely compared to other variables. The high relative deviations are mainly due to very low values of the total elongation in the high values of DoD. For these specimens, the necking phenomenon is almost not visible. Lastly, one needs to take into account the sensitivity of the total elongation for various factors, which was presented in Section 5.
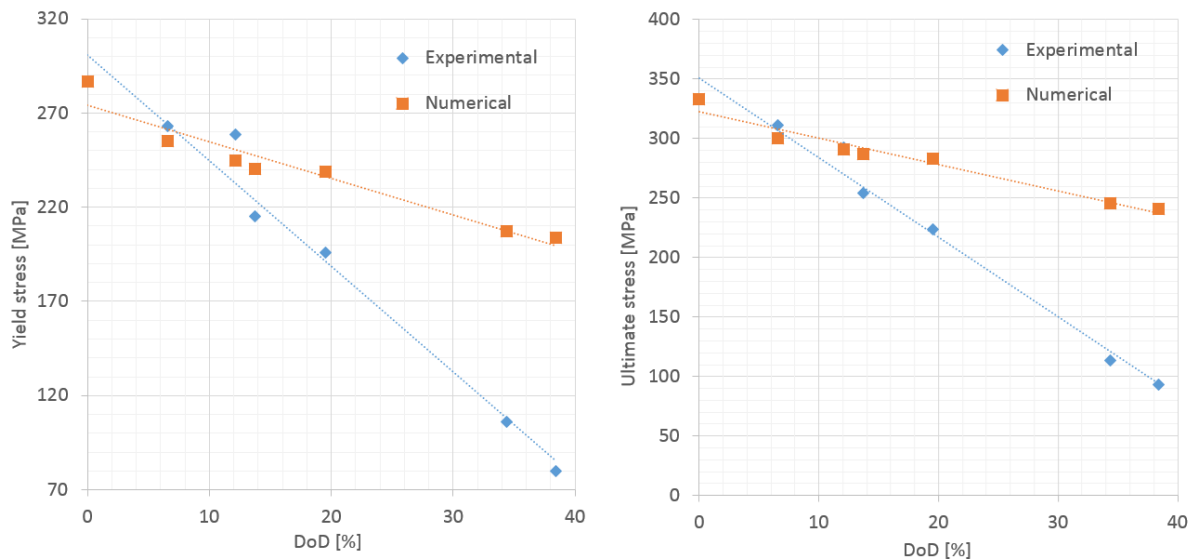

Figure 16. Yield (left) and ultimate (right) stresses in the function of DoD.
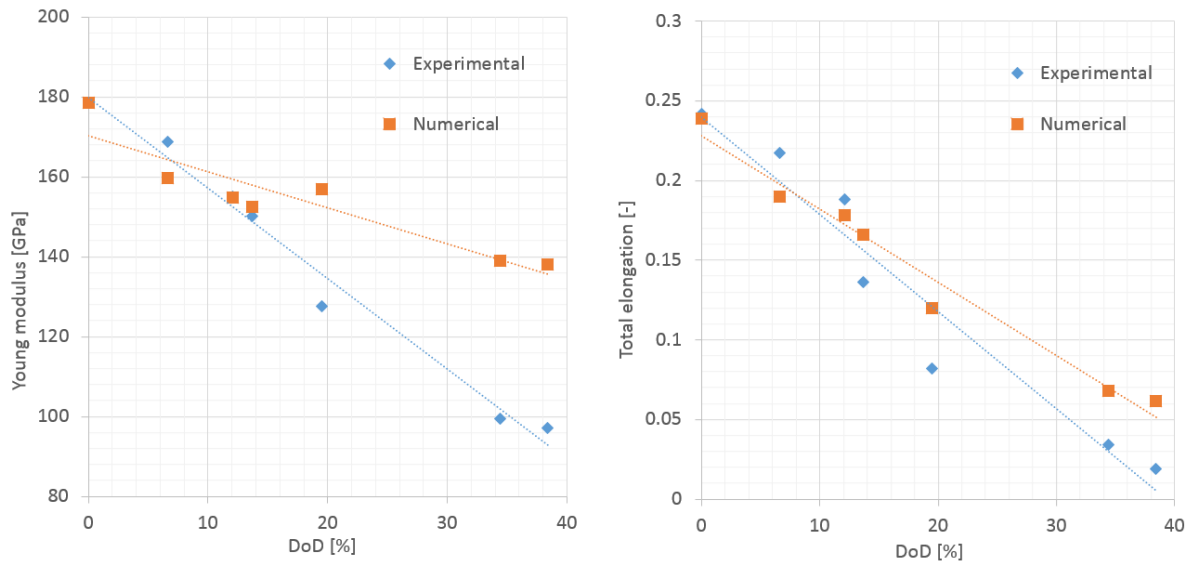
Figure 17. Young modulus (left) and total elongation (right) in the function of DoD.

Based on the presented results of the validation, it can be concluded that the corrosion degradation modelling with the use of the random approach predicts the mechanical properties reduction of very thin plates in the range between 0 and 15 % of DoD. Above this level, this approach significantly overestimates the mechanical properties. However, as it was discussed, the possible refinement of the mesh density can provide better results. The possible deviations can also be as a result of the lack of corrosion morphology information. In this case, only the maximum thickness and minimum cross-sectional area are provided for each specimen. Lastly, the deviations can be the result of natural variations of the mechanical properties in the case of the experiment as well as the sensitivity of random field modelling to the design parameters.

The comparison between experimental and numerical results of the stress-strain relationships are presented in Figures 18-20. One can notice that apart from the deviations, the shapes are very similar.
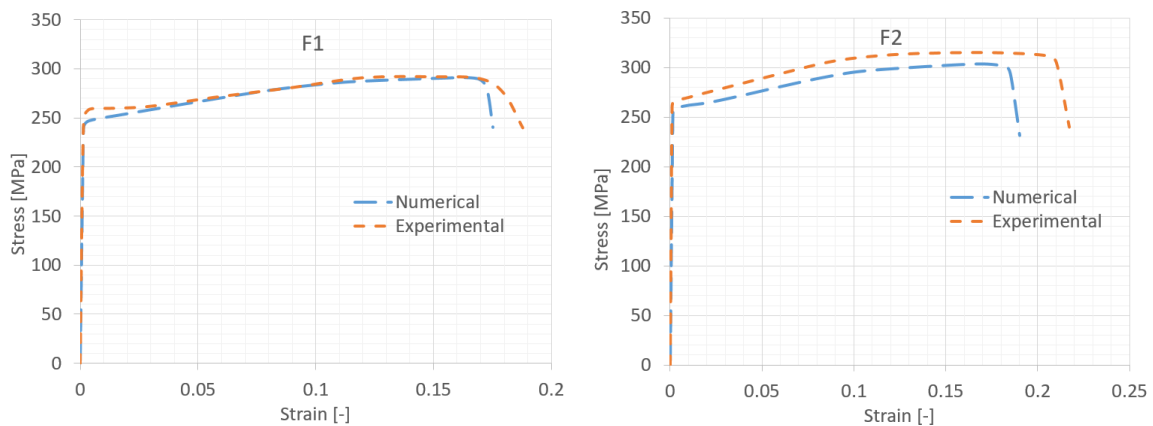

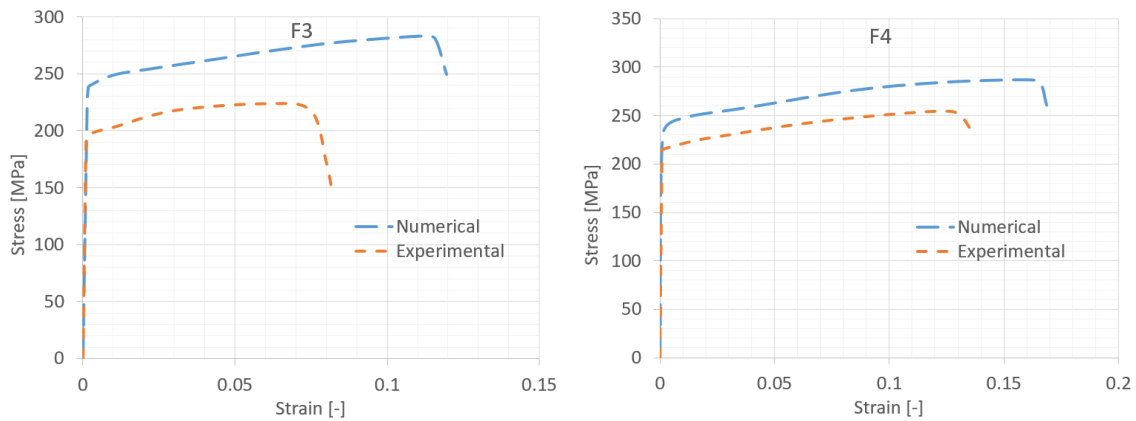Figure 18. Stress-strain curves of experimental and numerical results.

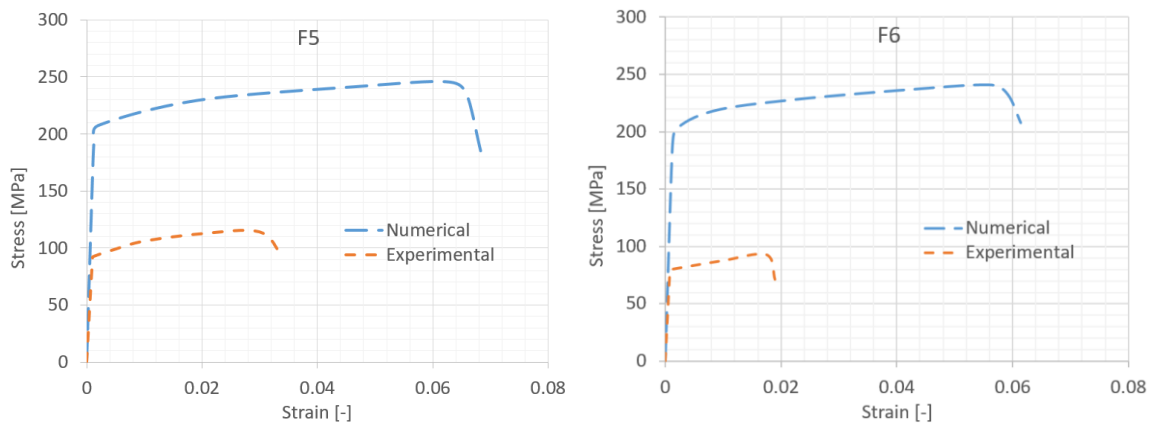Figure 19. Stress-strain curves of experimental and numerical results.

Figure 20. Stress-strain curves of experimental and numerical results.

7. Conclusions

The methodology developed here can be used in predicting the reduction of mechanical properties in terms of corrosion degradation. The developed methodology overestimates the mechanical properties only in the case of higher DoD. However, in operation, the highly corroded plates are usually replaced. The presented study confirms that the irregularities in the surface due to corrosion degradation are the main reason for the mechanical properties reduction. However, in the case of very high Degree of Degradation (above 15 %), other possible causes can impact the significant reduction of mechanical properties. The random field modelling of corrosion surfaces revelled to be a handy tool. The random field modelling can produce many samples, which is hard to obtain in reality due to the long duration of corrosion tests as well as challenging measurements of corrosion morphology. Due to the long duration of corrosion experiments, especially when the realistic corrosion rate wants to be generated, the random field modelling of corroded plates is economically and time-consuming justified. More experimental work is needed for further validation of the proposed methodology. Notably, the corroded specimens coming from the real marine environment would be valuable.

Nevertheless, different initial thicknesses need to be tested. Not only strength parameters such as yield stress, Young modulus and ultimate stress are reduced due to the corrosion process. The significant reduction of the total elongation transforms the material into a more brittle one. The energy absorption characteristics are also significantly reduced.

The sensitivity analysis revealed that the yield and ultimate stresses are non-dependent from random field parameters, and there are governed by minimum cross-sectional area. However, the total elongation and Young modulus are sensitive to those factors. The total elongation is subjected to the highest uncertainties, and it is the most sensitive output parameter. Thus, the higher deviations between numerical predictions and experimental results can be justified. The deviations between numerical and experimental results can originate from the uncertainties in the initial mechanical properties.

Additionally, the deviations can be as a result of a specific random field realisation as well as the sensitivity of the random field modelling to the design parameters. The element size of 0.25 mm was found to be good enough to represent the corrosion degradation morphology in the case of thin specimens. In a case of very thin plates, possible mesh refining can lead to better results in other to model more localised phenomena.

The reduction of mechanical properties can be different with different types of corrosion (atmospheric, marine, etc.) and thus, different corrosion types need to be investigated.

Acknowledgements

Sources

[1]   Garbatov Y, Guedes Soares C, Wang G. Nonlinear Time-Dependent Corrosion Wastage of Deck Plates of Ballast and Cargo Tanks of Tankers. J Offshore Mech Arct Eng 2006;129:48–55.

[2]   Melchers RE. Development of new applied models for steel corrosion in marine applications including shipping. Ships Offshore Struct 2008;3:135–44.

[3]   Paik JK, Thayamballi AK, Park Y Il, Hwang JS. A time-dependent corrosion wastage model for seawater ballast tank structures of ships. Corros Sci 2004;46:471–86.

[4]   Garbatov Y, Guedes Soares C, Parunov J, Kodvanj J. Tensile strength assessment of corroded small scale specimens. Corros Sci 2014;85:296–303.

[5]   Saad-Eldeen S, Garbatov Y, Guedes Soares C. Effect of corrosion degradation on ultimate strength of steel box girders. Corros Eng Sci Technol 2012;47:272–83.

[6]   Garbatov Y, Guedes Soares C, Parunov J. Fatigue strength experiments of corroded small scale steel specimens. Int J Fatigue 2014;59:137–44.

[7]   Teixeira AP, Ivanov LD, Guedes Soares C. Assessment of characteristic values of the ultimate strength of corroded steel plates with initial imperfections. Eng Struct 2013;56:517–27.

[8]   Wang Y, Wharton JA, Shenoi RA. Ultimate strength analysis of aged steel-plated structures exposed to marine corrosion damage: A review. Corros Sci 2014;86:42–60.

[9]   Fernandez I, Berrocal CG. Mechanical Properties of 30 Year-Old Naturally Corroded Steel Reinforcing Bars. Int J Concr Struct Mater 2019;13:9.

[10]   Kashani MM, Crewe AJ, Alexander NA. Nonlinear stress-strain behaviour of corrosion-damaged reinforcing bars including inelastic buckling. Eng Struct 2013;48:417–29.

[11] Zhang W, Shang D, Gu X. Stress-strain relationship of corroded steel bars. Tongji Daxue Xuebao/Journal Tongji Univ 2006;34.

[12] Li L, Mahmoodian M, Li CQ. Effect of corrosion on mechanical properties of steel bridge elements. 9th Int. Conf. Bridg. MAINTENANCE, Saf. Manag., 2018.

[13] Li L, Li C-Q, Mahmoodian M. Effect of Applied Stress on Corrosion and Mechanical Properties of Mild Steel. J Mater Civ Eng 2019;31:04018375.

[14] Wang Y, Xu S, Wang H, Li A. Predicting the residual strength and deformability of corroded steel plate based on the corrosion morphology. Constr Build Mater 2017;152:777–93.

[15] Nie B, Xu S, Yu J, Zhang H. Experimental investigation of mechanical properties of corroded cold-formed steels. J Constr Steel Res 2019;162:105706.

[16] Qin G, Xu S, Yao D, Zhang Z. Study on the degradation of mechanical properties of corroded steel plates based on surface topography. J Constr Steel Res 2016;125:205–17.

[17] Xu S, Zhang Z, Li R, Wang H. Effect of cleaned corrosion surface topography on mechanical properties of cold-formed thin-walled steel. Constr Build Mater 2019;222:1–14.

[18] Xu S, Zhang H, Wang Y. Estimation of the properties of corroded steel plates exposed to salt-spray atmosphere. Corros Eng Sci Technol 2019;54:431–43.

[19] Du YG, Clark LA, Chan AHC. Residual capacity of corroded reinforcing bars. Mag Concr Res 2005;57:135–47.

[20] Cairns J, Plizzari GA, Du Y, Law DW, Franzoni C. Mechanical properties of corrosion-damaged reinforcement. ACI Mater J 2005;102:256–64.

[21] Du YG, Clark LA, Chan AHC. Effect of corrosion on ductility of reinforcing bars. Mag Concr Res 2005;57:407–19.

[22] Palsson R, Mirza MS. Mechanical response of corroded steel reinforcement of abandoned concrete bridge. ACI Struct J 2002;99:157–62.

[23] Garbatov Y, Saad-Eldeen S, Guedes Soares C, Parunov J, Kodvanj J. Tensile test analysis of corroded cleaned aged steel specimens. Corros Eng Sci Technol 2018:1–9.

[24] Moreno E, Cobo A, Palomo G, González MN. Mathematical models to predict the mechanical behavior of reinforcements depending on their degree of corrosion and the diameter of the rebars. Constr Build Mater 2014;61:156–63.

[25] Fernandez I, Bairán JM, Marí AR. Mechanical model to evaluate steel reinforcement corrosion effects on σ-ε and fatigue curves. Experimental calibration and validation. Eng Struct 2016;118:320–33.

[26] Li D, Xiong C, Huang T, Wei R, Han N, Xing F. A simplified constitutive model for corroded steel bars. Constr Build Mater 2018;186:11–9.

[27] Nakai T, Matsushita H, Yamamoto N, Arai H. Effect of pitting corrosion on local strength of hold frames of bulk carriers (1st report). Mar Struct 2004;17:403–32.

[28] Ahmmad MM, Sumi Y. Strength and deformability of corroded steel plates under quasi-static tensile load. J Mar Sci Technol 2010;15:1–15.

[29] Appuhamy JMRS, Kaita T, Ohga M, Fujii K. Prediction of residual strength of corroded tensile steel plates. Int J Steel Struct 2011;11:65–79.

[30] Flaks VY. Correlation of pitting corrosion of aluminum plates and reduction of load-bearing capacity under tension. Sov Mater Sci 1978;14:75–8.

[31] Česen A, Kosec T, Legat A. Characterization of steel corrosion in mortar by various electrochemical and physical techniques. Corros Sci 2013;75:47–57.

[32] Wang Y, Xu S, Li H, Zhang H. Surface Characteristics and Stochastic Model of Corroded Structural Steel Under General Atmospheric Environment. Acta Metall Sin 2020;56:148–60.

[33] Xu S, Wang Y. Estimating the effects of corrosion pits on the fatigue life of steel plate based on the 3D profile. Int J Fatigue 2015;72:27–41.

[34] Kainuma S, Jeong Y-S, Ahn J-H. Investigation on the stress concentration effect at the corroded surface achieved by atmospheric exposure test. Mater Sci Eng A 2014;602:89–97.

[35] Pidaparti RM, Rao AS. Analysis of pits induced stresses due to metal corrosion. Corros Sci 2008;50:1932–8.

[36] Wang Y, Xu S, Li A. Flexural performance evaluation of corroded steel beams based on 3D corrosion morphology. Struct Infrastruct Eng 2020:1–16.

[37] Garbatov Y, Parunov J, Kodvanj J, Saad-Eldeen S, Guedes Soares C. Experimental assessment of tensile strength of corroded steel specimens subjected to sandblast and sandpaper cleaning. Mar Struct 2016;49:18–30.

[38] Woloszyk K, Kahsin M, Garbatov Y. Numerical assessment of ultimate strength of severe corroded stiffened plates. Eng Struct 2018;168:346–54.

[39] Garbatov Y, Tekgoz M, Guedes Soares C. Experimental and numerical strength assessment of stiffened plates subjected to severe non-uniform corrosion degradation and compressive load. Ships Offshore Struct 2017;12:461–73.

[40] Jankowski R, Walukiewicz H. Modeling of two-dimensional random fields. Probabilistic Eng Mech 1997;12:115–21.

[41] Górski J, Winkelmann K. Generation of random fields to reflect material and geometric imperfections of plates and shells. Shell Struct. Theory Appl. Vol. 4, CRC Press; 2017, p. 537–40.

[42] Górski J, Mikulski T, Oziębło M, Winkelmann K. Effect of geometric imperfections on aluminium silo capacities. Stahlbau 2015;84:52–7.

[43] Teixeira ÂP, Guedes Soares C. Ultimate strength of plates with random fields of corrosion. Struct Infrastruct Eng 2008;4:363–70.

[44] Garbatov Y, Guedes Soares C. Spatial Corrosion Wastage Modelling of Steel Plates Subjected to Marine Environments. Vol. 9 Offshore Geotech. Torgeir Moan Honor. Symp., American Society of Mechanical Engineers; 2017.

[45] Melchers R. Structural Reliability Analysis and Prediction. Chichester, UK: John Wiley & Sons Ltd; 2017.

[46] Ghanem RG, Spanos PD. Stochastic Finite Elements: A Spectral Approach. New York, NY: Springer New York; 1991.

[47] Li C, Der Kiureghian A. Optimal Discretization of Random Fields. J Eng Mech 1993;119:1136–54.

[48] Mathworks. Matlab R2019b 2019.

[49]   Constantine P. Random Field Simulation n.d.
         https://www.mathworks.com/matlabcentral/fileexchange/27613-random-field-simulation
         (accessed November 26, 2019).

[50]   ANSYS Inc. ANSYS LS-DYNA User's Guide 2019.

[51]   Bäker M. How to get meaningful and correct results from your finite element model 2018.

[52]   Wang Y, Xu S, Ren S, Wang H. An Experimental-Numerical Combined Method to Determine
         the True Constitutive Relation of Tensile Specimens after Necking. Adv Mater Sci Eng
         2016;2016:1–12.

[53]   ISO. Metallic materials - Tensile testing - Part 1: Method of test at room temperature. Int
         Stand ISO 6892-1 2009.

[54]   Scheider I, Brocks W, Cornec A. Procedure for the Determination of True Stress-Strain Curves
         From Tensile Tests With Rectangular Cross-Section Specimens. J Eng Mater Technol
         2004;126:70–6.

[55]   Kwesi Nutor R. Using the Hollomon Model to Predict Strain-Hardening in Metals. Am J Mater
         Synth Process 2017;2:1–4.

[56]   DNVGL-CG-0285. Ultrasonic thickness measurements of ships. DNV GL; 2016.

[57]   Cegla F, Gajdacsi A. Mitigating the effects of surface morphology changes during ultrasonic
         wall thickness monitoring. AIP Conf. Proc., 2016, p. 170001.

[58]   International Association of Classification Societies. Common Structural Rules (BC & OT).
         2018.

[59]   Daniel C. One-at-a-Time Plans. J Am Stat Assoc 1973;68:353–60.

[60]   Wu C-F, Hamada M. Experiments : planning, analysis, and optimisation. Wiley; 2009.

[61]   Li Z, Pasternak H. Experimental and numerical investigations of statistical size effect in S235JR
         steel structural elements. Constr Build Mater 2019;206:665–73.